Analysis of close approach and collision probability between operational satellites and/ or space debris

M. G. HALAWA*,[1], Yehia ABDEL-AZIZ[1], M. YOUSSEF[2]

*Corresponding Author
*,[1]National Research Institute of Astronomy and Geophysics (NRIAG),
11421-Helwan, Cairo, Egypt,
meirnagamal@nriag.sci.eg*, yehia@nriag.sci.eg
[2]Faculty of Science, Helwan University, Cairo, Egypt,
myousef7174@gmail.com

DOI: 10.13111/2066-8201.2020.12.3.9

Received: 22 April 2020/ Accepted: 24 July 2020/ Published: September 2020

Abstract: *In recent years, the number of space debris has increased significantly, which can threaten the safety of operational satellites. In this paper we developed an accurate model for active satellite protection from collision in order to determine close approaches between two objects (satellites and /or debris) using the Hoot's method and the time of close approach. We calculate the minimum relative distance considering J_2 and atmospheric drag perturbations, and compared it to the close approach distance. The Collision probability between two closed objects is calculated using Chan model and analyzed in a given time-scale to avoid any dangerous collision. We applied our models on the cataloged debris (more than 1000) resulted from the crash between Iridium 33 and Cosmos 2251; in addition, ten satellites from the Iridium satellites list at the same altitudes of the debris crowdie region are considered. The numerical results have shown one real case of close approach with high probability of collision that may threaten one of those active satellites.*

Key Words: *Close approach, Collision probability, Space debris, relative motion*

1. INTRODUCTION

Since the launch of the first Sputnik satellite in 1957, more than 5,560 successful launches of approximately 9,600 satellites in orbit around the Earth have taken place [1]; The ESA Space Debris Office estimates that by February 2020, approximately 5,500 of these satellites were still in space, while 2,300 are still in operation [1].
The total mass of all objects in Space reaches 8,800 tons distributed among 22,300 debris objects regularly tracked by Space Surveillance Networks [1]. The future prediction of close approaches between objects became very significant and essential. This is necessary both for the safety of Shuttle crews as well as for the protection of the operational satellites from inadvertent collisions.

Close approaches are defined as intervals of time when an object is within the exclusion zone of a satellite in the constellation. Once future close approaches have been identified, contingency plans can be enacted to reduce the probability of collision Woodburn and Dichmann [2]. However, the risk of a collision is likely to increase as the number of space missions increases. Due to the inadequate removal of the spacecraft from space upon

completion of its mission, spacecraft collisions become an increasing threat to the new spacecraft, according to Kessler et al [3].

The probability of a collision is defined as the probability that the miss distance between two objects is less than the sum of their safety-radii. The collision probability calculation is based on the integral of the probability distribution function with assumed nonlinear relative motion Alfano [4], Patera [5] or linear motion Alfano [6] and Foster [7]. Chen et al. [8] calculated the collision probability in terms of the relative position vectors or the conjunction geometries in circular orbit based on the closest approach analysis and estimation.

Hoots et al. [9] proposed an analytical method to calculate close approaches between two objects in orbits based on three filters, which candidate objects have to pass before a final determination of the close approach distance. Zheng and Wu [10] and Liu, Wang and Zhang [11] developed other analytical models improvement of the Hoots' method. Alfano and Negron [12], Alfano [13] developed a technique for modeling the distance separated between two objects using localized cubic polynomials.

Abdel-Aziz [14] and Abdel-Aziz and Abd El-Salam [15] developed an accurate model for predicting the positions of satellites and space debris based on a Hori-Lie method, and orbital evolution for short-term and the long-term propagation under the effects of all perturbing forces. Cao and Misra [16] developed a new series of linearized differential equations for describing the relative motion of satellites for elliptical orbits considered the J_2 disturbances and atmospheric drag effects. Abdul-Majid et al. [17] developed numerical techniques to predict the aerodynamic characteristic of satellites flying at LEO. Bakhtiari et al. [18] obtained the appropriate model for relative close/far distance hovering in low earth orbits for long time flight with consideration of zonal harmonics and Atmospheric drag perturbation.

Denenberg and Gurfil [19] developed a collision avoidance maneuver evaluation technique for a satellite cluster flight. Pastel [20] estimated the collision probabilities between satellite and debris by using the Adaptive Splitting Technique. Le May et al. [21] proposed 5 years duration of operational phase for one web and SpaceX constellations, the results indicate a high probability for collision occurrence.

In this work, we calculated the close approach distance (critical distance at which the object is at risk of collision) determined the closely spaced instants as a time of close approach. We solved nonlinear equation of motion considering J_2 and atmospheric Drag perturbations. In addition, we calculated the collision probability between the two closed objects. The numerical results and conclusions are introduced for different examples of operational satellites and/ or space debris.

2. CLOSE APPROACH ANALYSIS METHODS

The close approach analysis methods can be classified into the analytical method Hoots et al. [9] and the numerical method Alfano and Negron [11]. The Hoots method are based on geometrical analysis of the orbital elements, gain information about the close approach cases by the analytical methods. At certain time steps during a certain interval, the numerical methods are based on the orbital ephemeris of objects, or the position and velocity information from the orbital model. The relative position and close approach information are obtained by numerical processing methods.

2.1 The closest distance between the two conic sections

In this subsection, the constraint minimization problem is developed to determine the point of closest approach of any two conic sections.

The perpendicular distance (d) can be determined by:

$$d = L \sin I_R \sin u_R,$$
$$u_R = \theta + \omega, \quad \sin I_R = |\boldsymbol{\omega}_B \times \boldsymbol{\omega}_A| \tag{1}$$

where L is the orbit radius, I_R is the relative inclination angle between the two orbital planes, $\boldsymbol{\omega}_B$ and $\boldsymbol{\omega}_A$ are unit vectors normal to secondary and primary satellites' orbital planes, u_R is the argument of latitude relative to the intersection of the two orbit planes and θ is the true anomaly, ω is the argument of perigee.

The orbit radius is expressed as

$$L = \frac{a\,(1 - e^2)}{1 + e\cos\theta} \tag{2}$$

where a is the semi major axis and e is the eccentricity.

We want to find the time of close approach where the perpendicular distance d is equal to the separation distance D, $d = D$, substituting Eq. (2) in Eq. (1)

$$D = \frac{a(1 - e^2)\, sin\, I_R\, sin\, u_R}{1 + e\, cos\, \theta} \tag{3}$$

The problem is stated most generally by specifying a time of interest, let t_0 be the starting time and t_f is the final time, at the condition

$$R_{P\_max} - R_{a\_min} < D \tag{4}$$

where R_{P_max} is denoting the larger of the two perigees and R_{a_min} is denoting the smaller of the two apogees.

The two orbits are conjunct, so we have to check the second constraint (orbital path filter), to eliminate candidate objects whose orbital paths are independent of the satellite location, within the minimum allowed separation distance of the primary object.

The minimum distance occurs along the line of intersection, the relative line of nodes, of the two orbital planes.

The final filtration is based on crossing times for the two satellites and/or debris the intersection line of the two orbital planes.

The satellite will be in a region for a short period (t_0 - t_f) before and after it passes through the intersection line of the two orbital planes fig. (1).

An estimation of these times can be analytically obtained using the perpendicular distance d (Close approach distance) from one satellite to the other satellites or debris orbital plane.

If the perpendicular distance d is less than or equal to the relative separation distance between the two objects r_{rel} Hoot et al. [9]

$$d \le r_{rel} \tag{5}$$

$$r_{rel} = \sqrt{\boldsymbol{r}_B^2 - \boldsymbol{r}_A^2} \tag{6}$$

where $\mathbf{r}_A$, $\mathbf{r}_B$ are the position vector of primary and secondary satellite and/or space debris, respectively.

Then, the close approach occurs between the two objects. The Clohessy-Wiltshire [22] formula is used to determine the relative motion equations, assuming that two objects are subject to the central gravity field of the Earth.

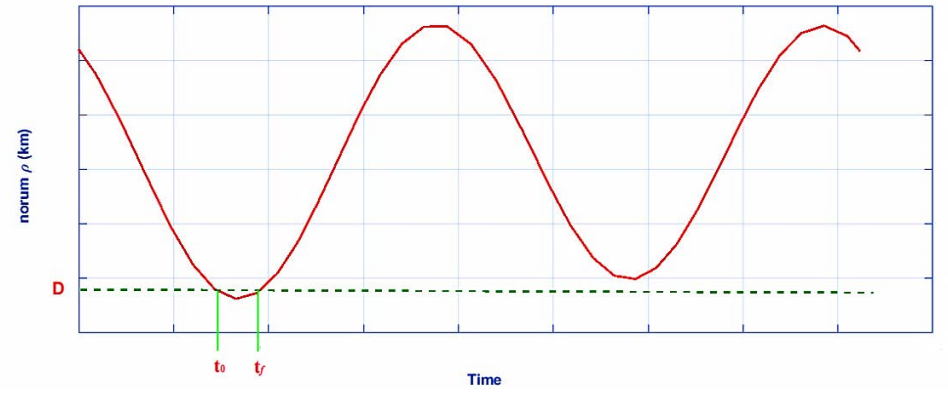

Fig. 1 - Relative motion and close approach distance between two objects [9].

2.2 Determine the time of closest approach

Time filter is used to compute the time intervals for each satellite when it is within the minimum allowed separation distance of the trajectory of the other object. The time intervals are based on the ranges of the relative argument of latitude computed in the orbit path filter and the related intervals for the primary satellite.

(A-N algorithm) Alfano and Negron method used a relative-distance function, for matching points and slopes in the combining functions Alfano and Negron [11]. This method used any distribution scheme, which allows the selection of a desired speed and accuracy.

Let $S(t)$ be the distance function which is the square of the distance and is given from relation

$$\begin{aligned} S(t) &= \mathbf{r}_{rel} \cdot \mathbf{r}_{rel} \\ \dot{S}(t) &= 2(\dot{\mathbf{r}}_{rel} \cdot \mathbf{r}_{rel}) \\ \ddot{S}(t) &= 2(\ddot{\mathbf{r}}_{rel} \cdot \mathbf{r}_{rel} + \dot{\mathbf{r}}_{rel} \cdot \dot{\mathbf{r}}_{rel}) \end{aligned} \tag{7}$$

Object close approaches occur whenever $S(t)$ is at a local minimum at the condition

$$\dot{S}(t) = 0,\ \ddot{S}(t) > 0 \tag{8}$$

The coefficients α_{cd} of the derivative function for the range-rate cubic polynomial equations $P_{cd}(\tau)$, cd=1,2,…, n which can be determined from Alfano and Negron [11], are:

$$\begin{aligned} P_c(\tau) &= \alpha_{c3}\tau^3 + \alpha_{c2}\tau^2 + \alpha_{c1}\tau + \alpha_{c0} \\ \alpha_{c0} &= S(t_n) \\ \alpha_{c1} &= \dot{S}(t_n)\Delta t \\ \alpha_{c2} &= -3S(t_n) - 2\dot{S}(t_n)\Delta t + 3S(t_{n+1}) - \dot{S}(t_{n+1})\Delta t \\ \alpha_{c3} &= 2S(t_n) + \dot{S}(t_n)\Delta t - 2S(t_{n+1}) + \dot{S}(t_{n+1})\Delta t \\ \Delta t &= t_{n+1} - t_n \end{aligned} \tag{9}$$

where τ varies from 0.0 to 1.0 and is an endpoint of the time interval containing the minima.

If the derivative of the function is used, the cubic splining still applies, simply use the first and second derivatives instead of the function and first derivative. Now, extract the real, distinct root (s), $\tau = \tau_{droot}$ of $Pcd(\tau)$ on the interval 0.0 to 1.0.

This is necessary to distinguish the results from the ellipsoidal function that we will examine shortly. If

$$\left.\frac{dP_{cd}(\tau)}{d\tau}\right|_{\tau=\tau_{droot}} > 0 \tag{10}$$

At local minimum range, the associated time of the close approach (t_{CA}) is

$$t_{CA}(\tau_{droot}) = t_n + \tau_{droot}\Delta t \tag{11}$$

3. NONLINEAR EQUATIONS OF RELATIVE MOTION

It is very important to include the relative motion between two objects for a more accurate calculation of the close approach. To achieve higher accuracy in calculating the relative motion between the two bodies, we use a nonlinear Cartesian coordinate system for the relative dynamics model under the effect of J_2 perturbation and atmospheric drag perturbation; more details can refer to Tealib et al. [23] for further details of derivatives of nonlinear dynamics model. A local-vertical-local-horizontal (LVLH) frame is attached to the primary satellite, see fig. (2). This coordinate frame rotates with the primary radius vector and is a convenient reference frame to describe the relative motion (x, y, z), the x-axis (radial direction) is directed from the center of the Earth towards the primary satellite, and the z-axis (cross-track) lies in the direction of the primary orbital angular momentum; the y-axis (along-track) completes the right-handed orthogonal triad Bakhtiari et al. [18].

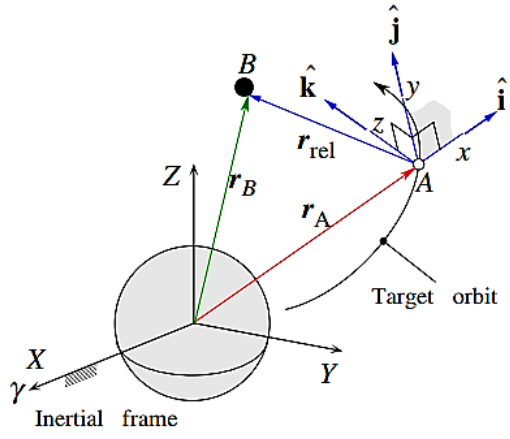

Fig. 2 - Local Vertical - Local Horizontal and Earth-Centered Inertial coordinates [24].

$$\dot{\boldsymbol{\theta}} = \frac{h}{r_B^2}\hat{k} = [0 \quad 0 \quad \dot{\theta}_z]^T, \quad \ddot{\boldsymbol{\theta}} = -\frac{2\dot{r}_B\dot{\theta}}{r_B}\hat{k} = [0 \quad 0 \quad \ddot{\theta}_z]^T \tag{12}$$

where h is the angular momentum for any object.

The equation of relative motion of the satellite and space debris under the effect of J_2 and atmospheric drag perturbations can be written as

$$\ddot{\mathbf{r}}_{rel} = \ddot{\mathbf{r}}_B - \ddot{\mathbf{r}}_A - \ddot{\boldsymbol{\theta}} \times \mathbf{r}_{rel} - \dot{\boldsymbol{\theta}} \times \left(\dot{\boldsymbol{\theta}} \times \mathbf{r}_{rel}\right) - 2\dot{\boldsymbol{\theta}} \times \dot{\mathbf{r}}_{rel} + \mathbf{a}_{J_2} + \mathbf{a}_{drag} \tag{13}$$

where $\mathbf{a}_{J2}$, $\mathbf{a}_{drag}$ are the accelerations due to the second zonal harmonic and atmospheric drag, respectively.

3.1 Nonlinear Relative J_2 Perturbations

The gravitational potential energy of the chief satellite can be written as Ginn [25].

$$\mathbf{U}_{J_2} = -\frac{\mu}{r_A} - \frac{3\mu J_2 R_e^2}{2r_A^3}\left(\frac{1}{3} - \sin^2\phi\right) = -\frac{\mu}{r_A} - \frac{3\mu J_2 R_e^2}{2r_A^3}\left(\frac{1}{3} - \frac{Z^2}{r_A^2}\right) \tag{14}$$

where R_e is Radius of the Earth, ϕ is the geocentric latitude of the satellite, μ is the gravitational parameter, Z is the Z-axis aligned with the Earth's rotation axis (ECI frame) and J_2 is the dominant harmonic in the oblateness perturbation. The accelerations acting on a satellite due to the J_2 perturbation can be derived from the potential functions in the desired coordinate system from Eq. (14). The accelerations in the inertial frame of reference, using Cartesian coordinates, are

$$\mathbf{a}_{J_2} = -\left[\frac{\partial U_{J_2}}{\partial X} i_X + \frac{\partial U_{J_2}}{\partial Y} i_Y + \frac{\partial U_{J_2}}{\partial Z} i_Z\right] = -\frac{3\mu J_2 R_e^2}{2r_A^4}\begin{Bmatrix}\left(1 - 3\frac{Z^2}{r_A^2}\right)\frac{X}{r_A}\\ \left(1 - 3\frac{Z^2}{r_A^2}\right)\frac{Y}{r_A}\\ \left(1 - 3\frac{Z^2}{r_A^2}\right)\frac{Z}{r_A}\end{Bmatrix} \tag{15}$$

The linear relative J_2 disturbance acceleration in the LVLH frame is given by Schweighart and Sedwick [26].

$$\mathbf{a}_{J_2} = \frac{6\mu J_2 R_e^2}{r_A^5}\begin{Bmatrix}(1 - 3\sin^2 i \sin^2\theta) & \sin^2 i \sin 2\theta & \sin 2i \sin\theta\\ \sin^2 i \sin 2\theta & -\frac{1}{4} - \sin^2 i\left(\frac{1}{2} - \frac{7}{4}\sin^2\theta\right) & -\frac{(\sin 2i \cos\theta)}{4}\\ \sin 2i \sin\theta & -\frac{(\sin 2i \cos\theta)}{4} & -\frac{3}{4} + \sin^2 i\left(\frac{1}{2} - \frac{5}{4}\sin^2\theta\right)\end{Bmatrix} \tag{16}$$

where i is the inclination angle of the chief satellite orbit.

4. THE ATMOSPHERIC DRAG PERTURBATION

Aerodynamic forces are quite significant at low altitudes and result in a large and undesired drift in the relative positions. Although these forces usually have a negative effect, for the relative station keeping it may be possible to use drag by the active actuation of aerodynamic panels, Reid and Misra [27]. The acceleration due to the atmospheric drag is given by Vallado [28].

$$\mathbf{a}_{drag} = -\frac{1}{2}\frac{C_D A}{m}\rho\|\mathbf{V}_{rel}\|\mathbf{V}_{rel} \tag{17}$$

where C_D is the drag coefficient of the spacecraft, A is the spacecraft projected cross-sectional area, ρ *is* the local atmospheric density, m is the spacecraft mass, and $\mathbf{V}_{rel}$ is the spacecraft velocity relative to the rotating atmosphere. The atmosphere of the Earth has a mean motion due to the rotation motion of the Earth, and it is approximated by the rotation rate of the Earth. The velocity with reference to the rotating atmosphere $\mathbf{V}_{rel}$ is given by Vallado [28]:

$$\mathbf{V}_{rel} = \mathbf{v}_s - \boldsymbol{\omega}_e \times \mathbf{r}_s \tag{18}$$

where the $\mathbf{r}_s$, $\mathbf{v}_s$ are vectors representing the absolute position and velocity of the spacecraft with respect to the center of the Earth and $\boldsymbol{\omega}_e = [0 \quad 0 \quad \omega_e]$ represents the Earth's angular velocity vector. To describe these drag effects in terms of Hill coordinates, the $\mathbf{V}_{rel}$ term must be described in the Hill frame. After some algebra, the expression for the velocity of a spacecraft relative to the rotating atmosphere in the Hill frame can be written as:

$$\mathbf{V}_{rel} = \begin{bmatrix} \dot{x} + \dot{r}_A - y(\dot{\theta} - \omega_e \cos i) - z\omega_e \cos\theta \sin i \\ \dot{y} + (r_A + x)(\dot{\theta} - \omega_e \cos i) + z\omega_e \sin\theta \sin i \\ \dot{z} + (r_A + x)\omega_e \cos\theta \sin i - y\omega_e \sin\theta \sin i \end{bmatrix} \tag{19}$$

5. COLLISION PROBABILITY

The probability density function (PDF) of the uncertainty of the separation between the primary and secondary is Chan [29].

$$f_3(x, y, z) = \frac{1}{\sqrt{(2\pi)^3 |C|}} e^{-\frac{1}{2}\bar{r}' C^{-1} \bar{r}} \tag{20}$$

where $\bar{r}$ radius of cross-section of circular torus and C is the combined covariance matrix in the encounter system, defined to be the sum of the individual covariance matrices for the case of independent or (less stringently) uncorrelated random variables. This covariance matrix gives the (PDF) of the uncertainty of the relative position of the satellites. The collision probability is

$$P = \iiint_V f_3(x, y, z) dx dy dz \tag{21}$$

where V is the volume swept by the sphere of radius r centered at the primary.

In the proximity of the encounter, the two objects trajectories are straight lines. The orbiting velocities are in the range of several kilometers per second, and the time spent in the encounter region is a fraction of a second or a few seconds at most, so that the gravitational force effects are negligible. This results in rectilinear motion essentially over a large region of standard deviations. Then, the volume swept out by the sphere of radius r is a long cylinder essentially extending along the y-direction from -∞ + ∞ to. Thus, instead of having to deal with a three-dimensional of PDF, we need only to consider the marginal two-dimensional of PDF. In the case of a joint Gaussian distribution of random variables, no tedious explicit integral evaluation needs to be performed. We assumed that $y = 0$ and appropriately change the multiplicative factor in the three-dimensional to obtain the desired result. Hence, the closest approach occurred at the primary cross the (x, z)-plane, and its relative position uncertainty is described by the following bivariate Gaussian of PDF Chan [29].

$$f(x, z) = \frac{r_a^2}{2\pi\sigma_x\sigma_z\sqrt{1 - \rho_{xz}^2}} e^{-\left[\left(\frac{x}{\sigma_x}\right)^2 - 2\rho_{xz}\left(\frac{xz}{\sigma_x\sigma_z}\right) + \left(\frac{z}{\sigma_z}\right)^2\right]/2(1-\rho_{xz}^2)} \tag{22}$$

where $r_a = \sqrt{x^2 + z^2}$ is combined hard-body radius and σ_x, σ_y, σ_z, ρ_{xz} are parameters in the combined covariance in the encounter plane

This expression can also be interpreted as the conditional of PDF for collision given that the primary object crosses the encounter plane. The collision probability in the encounter plane (x z) is given in two dimensions Peterson [30].

$$P = \frac{r_a^2}{2\pi\sigma_x\sigma_z\sqrt{1 - \rho_{xz}^2}} \iint_{A_a} exp\left\{-\frac{1}{2(1 - \rho_{xz}^2)} * \left[\left(\frac{x}{\sigma_x}\right)^2 - 2\rho_{xz}\left(\frac{xz}{\sigma_x\sigma_z}\right) + \left(\frac{z}{\sigma_z}\right)^2\right]\right\} dA_a \tag{23}$$

where P is the probability of collision and $A_a = \pi r_a^2$ is the cross-sectional area of the combined hard body radius.

6. NUMERICAL RESULTS AND DISCUSSIONS

In this section, we applied our (model) to determine the close approach distance using the Hoots method Eq. (3) and to calculate the time of close approach Eq. (11). The nonlinear differential equations of relative motion were solved using the 8th order Runge-Kutta method. We investigate the effects of perturbations due to the second zonal harmonic J_2 Eq. (16) and Drag force Eq. (17) to get high accuracy. These numerical simulations were performed using MATLAB©. Finally, we calculate the collision probability between two objects using the Chan model Eq. (23). First, we applied our models on the real example of a collision which occurred between Iridium-33 and Cosmos-2251 on 10 February 2009, as in Table 1.

Table 1. - Orbital elements for COSMOS 2251-IRIDIUM 33

Elements/ satellites	COSMOS 2251	IRIDIUM 33
NORAD ID	22675	24946
Perigee	772.8 km	781.0 km
Apogee	807.9 km	792.3 km
Inclination	74.0°	86.4°
Period	100.5 minutes	100.4 minutes
Semi-major axis	7161 km	7157 km

According to SOCRATES report [31], it predicted a close approach between Iridium 33 and Cosmos 2251 on 10 February 2009 at 15:00:00 UTC. And the actual collision occurred (based on the predicted time of the closest approach in the last SOCRATES report) at 16:55:59.806. The scenario was initialized to begin on 08 Feb 2009 at 00:00:00.00 UTC and run for a total of three days. This interval allows the time for approach and departure from the point of collision, as well as other close encounters at half-hour intervals. For the extension, propagated orbits were determined using both two-body dynamics, J_2 and Atmospheric drag perturbations. Note that the actual close approach occurred around 63 hours after the epoch, and the actual collision occurred around 65 hours after the epoch [31]. Fig. 3 and Table 2 show the close approach distance between Iridium 33 and Cosmos 2251 for three days with/ without perturbations. The numerical results show the close approach occurred after 61.268 hours from the epoch with no consideration of perturbation, with a miss distance of 62.01 km, as in fig 3.a. But if taking J_2 perturbation into consideration, this improves the results and reduces the error rate; the close approach occurred after 61.783 hours from the epoch with a miss distance of 65.53 km, as shown in fig. 3.b. Including the effect of the atmospheric drag has improved the results; the close approach occurred after 61.799 hours from the epoch with a miss distance of 65.55 km, see fig. 3.c.

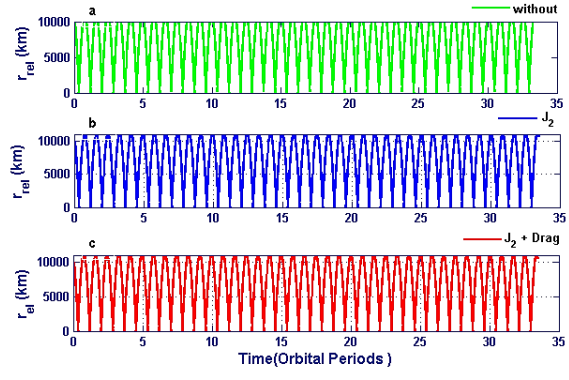

Fig. 3 - Propagation for three days before collision with/without perturbation

Table 2 - Close approach distance for 3-Day Propagation

	Close approach distance (km)	Time at the epoch	Time of Close approach
Without perturbation	62.01	8 Feb 00:00:00	10 Feb 13:16:44
J_2 only	65.53	8 Feb 00:00:00	10 Feb 13:44:31
J_2+drag	65.55	8 Feb 00:00:00	10 Feb 13:45:28

We studied the distribution of debris resulted from a collision between cosmos 2251 and iridium 33 debris catalogue [32]. Fig. 4 shows that the distribution of that debris at two different times, on 22/07/2012 the apogee and perigee concentrated in the altitude ranging from 1900 to 2050 km, and in an orbital period of 100 min. On 22/07/2018 we noticed that the change occurred in the distribution of debris, in meanwhile the apogee and perigee were concentrated from an altitude of 1950 to 2000 km, and from the orbital period from 90 to 101 minutes, so the debris get closer and the collision risk increases.

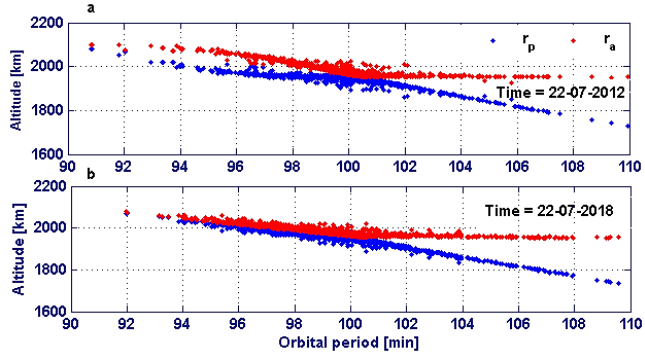

Fig. 4 - Generated debris Apogee and perigee catalogue over the orbital period at two different times.

Fig. 5 shows the distribution of that debris on 22/07/2018 with a semi-major axis, eccentricity and inclination, respectively. The debris is densely dispersed in the range of the semi-major axis from 1950 to 2000 km, crowded as well at a range of eccentricity from 0.002 to 0.004 , at two different inclination angles 86 degree for Iridium debris and 74 degree for cosmos debris. So we study the close approach for some active satellite at the same region.

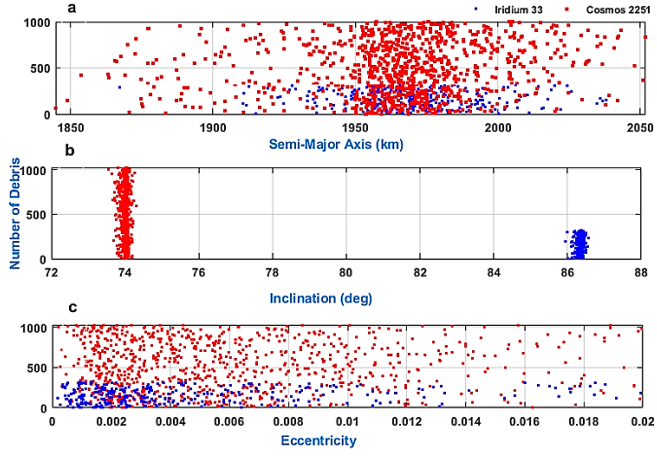

Fig. 5 - The distribution between semi-major axis, Inclination and Eccentricity verses number of debris catalogue at 22/07/2018

We applied our models on the debris resulted from Iridium33 and Cosmos2251 crash catalogue (ID No 24946 - 40993) [32] and in addition on ten active satellites from the Iridium satellites listed in Table 3. at crowdie region of debris.

We investigate the conjunction between the satellites' orbits and the debris orbits using the condition in Eq. (4). We suppose that the close approach distance is 5 km and we apply the condition in Eq. (4) for analyzing the conjunction between the satellites in Table 3.

Step1. In the filtration process we clarified the number of conjunctions occurred between the orbit of the active satellite and the orbits of the surrounding debris in a single day. Table 4. has shown how dangerous can be the existence of the active satellites in this crowded region of space debris.

Step2. We obtained a close approach by applying the second condition in Eq. (5). The numerical results from Table 5. show the filtration output, and the debris closest to the active satellites and the collision probability of these debris with the active satellites.

Table 3. - Two Line Elements for Iridium satellites list [32].

0 IRIDIUM 131 1 43079U 17083K 18203.79622436 +.00000043 +00000-0 +83726-5 0 9993 2 43079 086.3968 088.2613 0002386 085.4976 274.6492 14.34216106030398
0 IRIDIUM 153 1 43078U 17083J 18203.73255951 +.00000201 +00000-0 +20804-4 0 9993 2 43078 085.5938 061.7563 0012516 228.0769 131.9387 14.83790703031377
0 IRIDIUM 141 1 43077U 17083H 18203.80892287 +.00000055 +00000-0 +12612-4 0 9994 2 43077 086.3962 088.2630 0002223 093.3037 266.8413 14.34218277030460
0 IRIDIUM 137 1 43076U 17083G 18203.81526836 +.00000073 +00000-0 +18980-4 0 9992 2 43076 086.3967 088.2724 0001812 099.4972 260.6428 14.34217477030465
0 IRIDIUM 32 1 24945U 97051B 18203.90108238 +.00000146 +00000-0 +44945-4 0 9992 2 24945 086.3971 119.6390 0001708 083.7499 276.3891 14.34218984091858
0 IRIDIUM 151 1 43074U 17083E 18203.83430065 +.00000063 +00000-0 +15432-4 0 9998 2 43074 086.3964 088.2562 0001853 094.8013 265.3394 14.34217384030438
0 IRIDIUM 130 1 43073U 17083D 18203.78988159 +.00000062 +00000-0 +14974-4 0 9992 2 43073 086.3971 088.2748 0002243 089.3909 270.7543 14.34215863030401
0 IRIDIUM 116 1 43072U 17083C 18203.75184707 +.00000073 +00000-0 +19040-4 0 9996 2 43072 086.3962 088.2996 0001852 091.1539 268.9869 14.34217756030458
0 IRIDIUM 138 1 43071U 17083B 18203.78355119 +.00000057 +00000-0 +13383-4 0 9991 2 43071 086.3952 088.2533 0002365 087.7346 272.4121 14.34218087030426
0 IRIDIUM 135 1 43070U 17083A 18203.82795345 +.00000064 +00000-0 +15680-4 0 9994 2 43070 086.3963 088.2477 0001788 073.1411 286.9981 14.34218070030442

Table 4. - The conjunction occurrence between resulted of debris &10 nearby satellites 22/07/2018.

Satellite	Number of conjunction
IRIDIUM 131-43079	137
IRIDIUM 153-43078	136
IRIDIUM 141-43077	139
IRIDIUM 135-43070	138
IRIDIUM 137-43076	163
IRIDIUM 151-43074	142
IRIDIUM 130-43073	138
IRIDIUM 116-43072	142
IRIDIUM 138-43071	138
IRIDIUM 32-24945	134

Table 5. - Close approach and Collision probability for the satellite list.

The first object (Satellite)	Second object (Debris)	Close approach distance (km)	Time of close approach	Collision probability
IRIDIUM 131 (43079)	COS 2251 DEB(33758)	11.119858	22-7-2018 19:35:3	1.398414e-10
	IRID 33 DEB (33858)	0.528403	22-7-2018 19:25:46	2.496753e-19
IRIDIUM 153(43078)	COS2251 DEB(33936)	29.869427	22-7-2018 18:8:32	6.541166e-27
IRIDIUM 141(43077)	COS 2251 DEB(34383)	24.923234	22-7-2018 19:38:38	7.261912e-38
	IRID 33 DEB (34486)	13.065412	22-7-2018 19:47:61	2.714012e-23
IRIDIUM 135(43076)	IRID 33 DEB (35925)	23.729329	22-7-2018 19:38:23	4.730263e-21
	COS 2251 DEB(35960)	1.524875	2-7-2018 19:43:24	3.668978e-11
	COS 2251 DEB(33819)	4.3424	22-7-2018 21:6:13	2.356125e-08
IRIDIUM 137(43075)	COS 2251 DEB(34401)	24.913975	22-7-2018 19:46:57	6.455744e-24
	COS 2251 DEB(34464)	2.758090	22-7-2018 19:49:25	7.401458e-11
	IRID33 DEB (34488)	21.990342	22-7-2018 19:56:36	2.663528e-24
IRIDIUM 151(43075)	COS 2251 DEB(34624)	14.945013	22-7-2018 20:18:55	3.951464e-21
	IRID 33 DEB (43074)	19.801501	22-7-2018 20:20:23	2.347236e-34
IRIDIUM 130 (43073)	COS2251 DEB (34968)	11.152720	22-7-2018 19:15:38	1.572799e-64
	COS2251 DEB (34967)	5.764156	22-7-2018 19:6:3	5.568754e-13

The first object (Satellite)	Second object (Debris)	Close approach distance (km)	Time of close approach	Collision probability
IRIDIUM 116 (43072)	IRID33 DEB (35739)	4.622807	22-7-2018 18:26:15	7.750496e-21
	COS2251 DEB (36367)	24.494242	22-7-2018 18:21:25	2.684853e-24
IRIDIUM 32 (24945)	IRID33 (24946)	2.932	22-7-2018 22:1:28	1.51415e-08
	IRID33 DEB (33850)	5.607882	22-7-2018 22:51:10	6.148469e-10
	IRID33 DEB(33859)	5.145727	22-7-2018 22:51:31	6.015149e-43

We found a real case of close approach between one of these satellites and a space debris, with the highest collision probability compared to the rest of the objects. Which is the satellite IRIDIUM 32 (ID 24945) versus the debris IRIDIUM 33(ID 24946) shown in Table 5. The numerical results have shown that the value of the relative minimum distance is 1.175 km, and the close approach distance is 2.932 km and the time of close approach at 22/07/2018 when the initial time is 22:01:25 while the final time is 22:02:25. The probability of collision in that case is 1.51415e-08.

In fig. 6 the blue curve represents the relative position between the satellite IRIDIUM 32 and debris IRIDIUM 33 versus time, the red line D represents the calculated close approach distance.

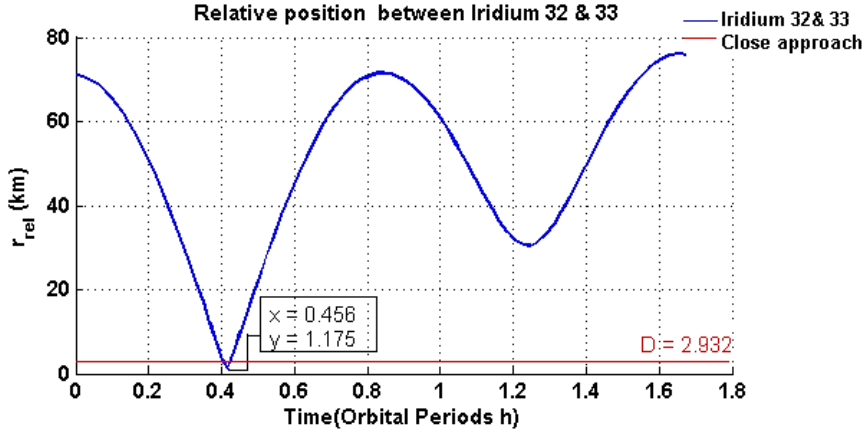

Fig. 6 - The Close approach between the satellite IRIDIUM 32 and debris IRIDIUM 33

It was very important to include the effect of J_2 and atmospheric drag perturbation on the relative position for different time periods. Fig. 7 shows that the change in norm relative of IRIDIUM 32 & 33 propagated at different times. The drift in minimum norm relative position propagation of IRIDIUM 32 & 33 is about 165 m for one day before close occurrence without perturbation, and about 3.225 km with J_2 and atmospheric drag propagation as in Fig. 7-a. For two days propagation before close occurrence, the drift in minimum norm relative position without perturbation becomes about 800 m and 4.2 km with perturbation effects as in Fig. 7-b. However, the value of drift changes to 1.5 km for three days before close occurrence without perturbation, and 7 km with J_2 and atmospheric drag perturbation as in Fig. 7-c. With propagation for a week before close occurrence the drift in norm relative position without perturbation is 5.9 km, and about 11 km under the perturbation effects as in Fig. 7-d.

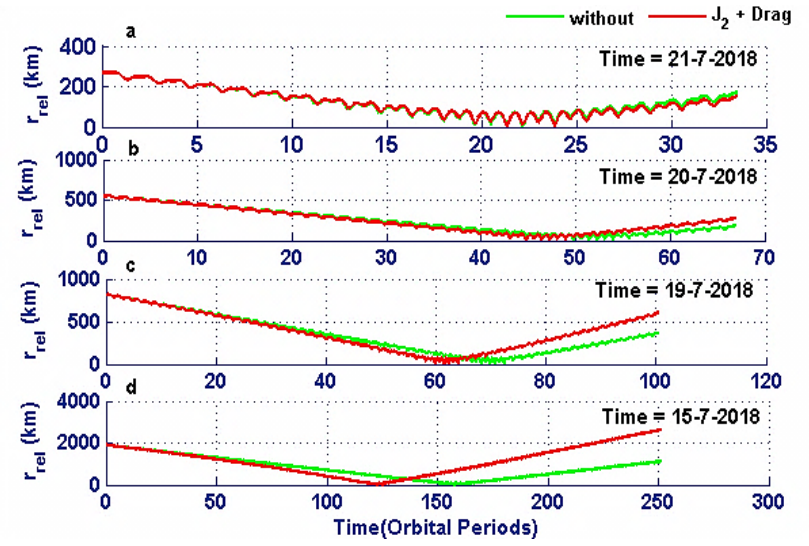

Fig. 7 - Relative motion of iridium 32&33 propagated for a day, two days, three days and a week before close occurrence

Figs. (8, 9) show that the change in trajectory, In-plan and out- plan of IRIDIUM 32 & 33 propagated at different times. The relative motion in the along-track direction is affected by the largest navigation errors, if the along-track is compared with radial and cross-track, due to the uncertainties associated with the characteristics of the upper atmosphere. The satellite orbit dynamics in along-track direction are highly coupled due to the Kepler equations. So, any maneuver execution errors and cross-coupling will cause a rapidly varying along-track motion with an offset that accumulates over time.

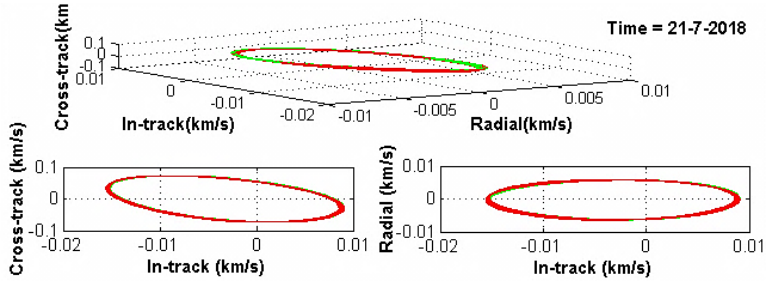

Fig. 8 - Drift in trajectory, In-plan and out- plan of IRIDIUM 32 & 33 propagated one day before close occurrence

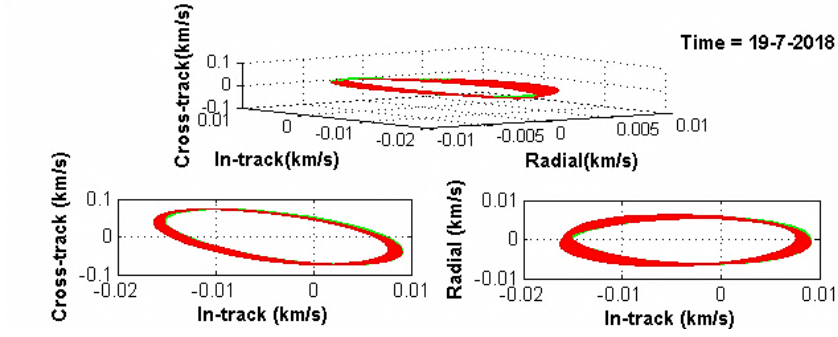

Fig. 9 - Drift in trajectory, In-plan and out- plan of IRIDIUM 32 & 33 propagated three days before close occurrence

7. CONCLUSIONS

We developed an accurate model to calculate the close distance, the time of close approach and relative motion considering J_2 and atmospheric drag perturbations. We applied our models on the actual collision that occurred on 10 February 2009 between Iridium33 and Cosmos2251. Then we studied the distribution of debris resulted from Iridium33 and Cosmos2251 crash, in addition to ten active satellites from iridium satellites listed at the same altitudes of the debris crowdie region. The filtration processes found one real case of close approach with high collision probability threatening one of those active satellites. This indicates the extent of the threat to the active satellites in the space debris accumulation areas and the need to avoid launching new satellites near these areas.

REFERENCES

[1] * * * ESA's Space Debris Office, 2020, *Space debris by the numbers* [WWW Document], ESA website URL http://www.esa.int/Our_Activities/Operations/Space_Debris/Space_debris_by_the_numbers

[2] J. Woodburn and D. Dichmann, *Determination of Close Approaches for Constellations of Satellites*, In Mission Design & Implementation of Satellite Constellations (pp. 337-345), Springer, Dordrecht, 1998.

[3] D. J. Kessler, N. L. Johnson, J. C. Liou and M. Matney, The kessler syndrome: implications for future space operations, *Advances in the Astronautical Sciences*, **137**(8), 2010.

[4] S. Alfano, Addressing nonlinear relative motion for spacecraft collision probability, in *Proc. AIAA/AAS Astrodyn. Specialist Conf. Exhib.*, p. 6760.. DOI: 10.2514/6.2006-6760, Aug. 2006.

[5] R. P. Patera, General method for calculating satellite collision probability, *J. Guide., Control, Dyn.*, vol. **24**, no. 4, pp. 716–722, 2001.

[6] S. Alfano, A numerical implementation of spherical object collision probability, *J. Astron. Sci.*, vol. **53**, no. 1, pp. 103–109, 2005.

[7] J. L. Foster, *The analytic basis for debris avoidance operations for the international space station*, in Proc. 3rd Eur. Conf. Space Debris, Darmstadt, Germany, vol. **473**, pp. 441–445, Mar. 2001.

[8] L. Chen, X. Z. Bai, Y. G. Liang, and K. B. Li, Calculation of collision probability, in *Orbital Data Applications for Space Objects*, Singapore Springer, pp. 135–183, 2017.

[9] F. R. Hoots, L. L. Crawford and R. L. Roehrich, An Analytic Method to Determine Future Close Approaches Between Satellites, Celestial Mechanics, Vol. **33**, pp. 143-158, 1984.

[10] Q. Y. Zheng and L. D. Wu, A computation method to warn the collision event between a space probe and debris, *Acta Astronomica Sinica*, **45**, pp.421-427, 2004.

[11] J. Liu, R. L. Wang, H. B. Zhang and Z. Xiao, Space debris collision prediction research, *Chin J Space Sci.*, **24**, no. 6: 462-469, 2004.

[12] S. Alfano and D. Jr. Negron, Determining Satellite Close Approaches, *The Journal of the Astronautical Sciences*, Vol. **41**, No. 2, pp. 217-225, April-June 1993.

[13] S. Alfano, Determining satellite close approaches, part 2, *Journal of the Astronautical Sciences*, **42**, pp.143-152, 1994.

[14] Y. A. Abdel-Aziz, An analytical theory for avoidance collision between space debris and operating satellites in LEO, *Applied Mathematical Modelling*, **37**(18-19), pp.8283-8291, 2013.

[15] Y. A. Abdel-Aziz and F. A. El-Salam, An efficient algorithm for orbital evolution of artificial satellite, *Applied mathematics and computation*, **191**(2), pp.415-428, 2007.

[16] L. Cao and A. K. Misra, Linearized J2 and atmospheric drag model for satellite relative motion with small eccentricity, *Proceedings of the Institution of Mechanical Engineers, Part G: Journal of Aerospace Engineering*, **229**(14), pp.2718-2736, 2015.

[17] Abdul-Majid, M. N. Owais and M. N. Qureshi, Aerodynamic Drag Computation of Lower Earth Orbit (LEO) Satellites, *Journal of Space Technology*, Vol. **8**, No. 1, July 2018.

[18] M. Bakhtiari, K. Daneshjou and M. Fakoor, Relative hovering analysis about an elliptical perturbed orbit with consideration of dynamic air drag and oblate earth, *Aerospace Science and Technology*, **70**, pp.286-299, 2017.

[19] E. Denenberg and P. Gurfil, Debris avoidance maneuvers for spacecraft in a cluster, *J. Guide., Control, Dyn.*, vol. **40**, no. 6, pp. 1428–1440, 2017.

[20] R. Pastel, Estimating satellite versus debris collision probabilities via the adaptive splitting technique,' in *Proc. 3rd Int. Conf. Comput. Modeling Simulation*, Mumbai, India, pp. 1–6, 2011.

[21] S. Le May, S. Gehly, B. A. Carter and S. Flegel, 'Space debris collision probability analysis for proposed global broadband constellations, *Acta Astronaut.*, vol. **151**, pp. 445–455, Oct. 2018.
[22] W. H. Clohessy and R. S. Wiltshire, Terminal Guidance System for Satellite Rendezvous, *Journal of the Aerospace Sciences*, Vol. **27**, No. 9, pp. 653-658, 1960.
[23] S. K. Tealib, Y. A. Abdel-Aziz, M. E. Awad, K. I. Khalil and M. Radwan, Semi-Analytical Solution for Formation Flying Spacecraft Subject to Electromagnetic Acceleration, *Universal Journal of Mechanical Engineering*, **8**(1): 41-50, 2020.
[24] H. D. Curtis, *Orbital mechanics for engineering students*, Butterworth-Heinemann, 2013.
[25] J. S. Ginn, *Spacecraft Formation Flight: Analysis Of The Perturbed J2-modified Hill-Clohessy-Wiltshire Equations*, 2007.
[26] S. A. Schweighart and R. J. Sedwick, High-fidelity linearized J model for satellite formation flight, *Journal of Guidance, Control, and Dynamics*, **25**(6), pp.1073-1080, 2002.
[27] T. Reid and A. K. Misra, Formation flight of satellites in the presence of atmospheric drag, *Journal of Aerospace Engineering*, **3**(1), p.64, 2011.
[28] D. A. Vallado, *Fundamentals of Astrodynamics and Applications*, ISBN: 978-11881883180, 2013.
[29] K. Chan, Short-term vs. long-term spacecraft encounters, *In AIAA/AAS astrodynamics specialist conference and exhibi*t (p. 5460), August 2004.
[30] G. E. Peterson, Maneuver selection for probability reduction of near-circular orbit conjunctions, *In AIAA/AAS Astrodynamics Specialist Conference and Exhibit*, Monterey, CA, 2002.
[31] T. S. Kelso, Analysis of the iridium 33 cosmos 2251 collision, 2009, Amos2009.pdf.
[32] * * * https://www.space-track.org/#/tle.